photonics

MDPI

Article

Illustrations of Bessel Beams in *s*-Polarization, *p*-Polarization, Transverse Polarization, and Longitudinal Polarization

A. Srinivasa Rao [1,2,3]

[1] Graduate School of Engineering, Chiba University, Chiba 263-8522, Japan; asvrao@chiba-u.jp
[2] Molecular Chirality Research Centre, Chiba University, Chiba 263-8522, Japan
[3] Institute for Advanced Academic Research, Chiba University, Chiba 263-8522, Japan

Abstract: The generation of Bessel beams (BBs) and their characterization in a wide range of the electromagnetic spectrum are well established. The unique properties of BBs, including their non-diffracting and self-healing nature, make them efficient for use in material science and engineering technology. Here, I investigate the polarization components (*s*-polarization, *p*-polarization, transverse polarization, and longitudinal polarization) created in scalar BBs owing to their conical wave front. For emphasis, I provide a theoretical analysis to characterize potential experimental artifacts created in the four polarization components. Further, I provide a brief discussion on how to prevent these artifacts in scalar BBs. To my knowledge, for the first time, I can generate vector BBs in *s*-polarization and *p*-polarization via the superposition of two orthogonally polarized scalar BBs. This method of generation can provide the four well-known types of vector modes categorized in the V-point phase singularity vector modes. I suggest a suitable experimental configuration for realizing my theoretical results experimentally. The present analysis is very practical and beneficial for young researchers who seek to utilize BBs in light applications of modern science and technology.

Keywords: Bessel beam; *p*-polarization; *s*-polarization; vector Bessel beam; Fresnel reflection; radial vector beam; azimuthal vector beam; orbital angular momentum

Citation: Rao, A.S. Illustrations of Bessel Beams in *s*-Polarization, *p*-Polarization, Transverse Polarization, and Longitudinal Polarization. *Photonics* **2023**, *10*, 1092. https://doi.org/10.3390/photonics10101092

Received: 12 August 2023
Revised: 13 September 2023
Accepted: 25 September 2023
Published: 29 September 2023

1. Introduction

Bessel beams (BBs) were first introduced and experimentally demonstrated by Durnin et al. [1,2]. These beams are non-diffracting and self-healing solutions to the Maxwell wave equation. After the first demonstration of Bessel beams, multiple mathematical models were used to theoretically suggest various kinds of BBs [3–6]. In any type of BB, while the zero-order BB has no helical wave front, higher-order BBs contain a helical wave front and the helicity increases when their order is increased, in a similar fashion to Laguerre–Gaussian beams. The helicity or twist in the wave front of a BB is quantified via the orbital angular momentum (OAM) quantum number or topological charge. Therefore, the order of the BB is referred to as the OAM quantum number. Mathematically, one can easily realize ideal BBs. Ideal BBs have infinite energy and spatial extent, and cannot be experimentally realized. However, well-developed modern experimental configurations can produce high-quality quasi-BBs over a wide range of the wavelength spectrum, whose energy and spatial extent are finite, via using diffractive optical elements (an annular aperture, spatial light modulator, axicon, etc.) in combination with nonlinear wave-mixing [7–9]. Wavelength-versatile BBs with three-dimensional tunable shapes have been experimentally generated in a wide range of the electromagnetic spectrum and have seen tremendous applications in modern science and engineering technology owing to their unique propagation properties. For instance, a long, needle-like structure with low-intensity side rings of a zero-order BB is used for the rapid volumetric imaging of biological tissues in the presence of two-photon absorption and three-photon absorption [10]. The signal to background noise in bio-imaging due to BBs' side lobes can be successfully suppressed through multi-photon

absorption. The non-diffraction and self-healing nature of BB is used for trapping microparticles in multiple planes along the beam's axis [11]. The distortion created in the BB due to the trapping of particles in the first plane will be self-healed, and the same beam can be used to trap particles in the second plane. It is also noted that the separation between the two trapping planes must be greater than the self-healing length of the BB. The long depth of focus with a self-healing BB of the zero-order can easily penetrate into a material of a constant size. This significant property is used to create micro- and nanostructures inside materials [12]. The central dark core with a helical wave front, which is formed in higher-order BBs, can create micro-size diameter fibers of a few centimeters in length in the materials via photo-polymerization [13]. Also, the orbital angular momentum of higher-order BBs can be used for free-space and underwater optical communications [14].

When it comes to the properties of BBs, the propagation of individual waves in a BB is completely different from the beam-axis direction. Here, the individual waves of a BB propagate in a conical shape to produce their self-healing and non-diffractive nature. This conical shape splits the amplitude of a BB into four components: *s*-polarization, *p*-polarization, transverse polarization, and longitudinal polarization. These four components are present in every BB, irrespective of its order and cone angle, and play pivotal roles in the applications of BBs. For example, when a BB propagates from one medium to another medium, the reflection and transmission coefficients are different for *s*-polarization and *p*-polarization [15], and this leads to distortions in their transverse intensity distributions [16–24]. Thus, these distortions can produce significant errors in the abovementioned applications of BBs. The plasmon resonance excitation of evanescent BBs can be created via the tight focusing of BBs. The tight focusing condition will create a significant longitudinal electric field component in the BB. Hence, in the plasmon resonance excitation of evanescent BBs, we can see a non-uniform intensity distribution along the transverse polarization and longitudinal polarization of scalar BBs [25,26]. BBs, which are directly generated from a laser cavity with an intra-cavity short-focal-length lens, have asymmetry in their transverse intensity distribution due to their polarization-dependent reflection coefficient [27]. In light–matter interactions, the interaction of the material with light is different for *s*-polarization and *p*-polarization [28–31], and this leads to the degradation of the material's processing quality and ambiguity in the investigation of the material's properties. The absorption of some of the optical materials is very sensitive to polarization [32,33], leading to asymmetry in absorption-based applications.

As I mentioned above, *s*-polarization, *p*-polarization, transverse polarization, and longitudinal polarization have played significant roles in the applications and propagation of BBs. Hence, it is necessary to understand the polarization properties of BBs before utilizing them in applications. Here, I provide a simple theoretical analysis to understand the illustrations of a BB in *s*-polarization, *p*-polarization, transverse polarization, and longitudinal polarization. All the calculations carried out herein consider that the BB propagates normally to the material's surface (normal incidence). Further, my investigation is extended to generate vector BBs from the superposition of two orthogonally polarized scalar BBs. To the best of my knowledge, for the first time, I report the generation of cylindrical vector modes in *s*-polarization and *p*-polarization. The outcomes of the present work open the door to further experimental and theoretical investigations of other structured laser modes and thereby unlock the potential of these kinds of fields for future applications such as material processing, bio-imaging, and optical communication.

The article is organized as follows: The motivation and background of the work are discussed in the introduction (Section 1). In Section 2, I describe a general theory on the splitting of the field amplitude of BBs in *s*-polarization, *p*-polarization, transverse polarization, and longitudinal polarization and its illustrations. Subsequently, Section 3 provides a discussion of the results drawn from theoretical expressions and numerical simulations. I suggest a suitable experimental setup for understanding my theoretical results. Finally, I present my conclusions in Section 4.

2. Theory

Suppose a BB is propagating along the z-axis and is polarized in the yz-plane (Figure 1). The angle θ is directed from the z-axis to the xy-plane, and the angle ϕ lies in the xy-plane and is directed from the x-axis to the y-axis. Then, the conical shape propagation of scalar BB divides its optical field amplitude into three components along the x, y, and z directions: E_x, E_y, and E_z. Thus, the optical field of the scalar BB E has an explicit form of E (x, y, z, ϕ, θ). Similarly, the propagation vector k of the individual waves on the Bessel cone can have three components k_x, k_y, and k_z along the respective x-, y-, and z-axes. The electric field and k-vector distributions of the scalar BB in three dimensions are given in Figure 1a. The projections of the k-vector on the z-axis and the xy-plane are given by $k_z = k\cos\theta$ and $k_r = k\sin\theta$, respectively. Further, k_r is projected onto the x-axis and the y-axis as $k_x = k\sin\theta\cos\phi$ and $k_y = k\sin\theta\cos\phi$, respectively. Also, the electric field oscillating perpendicular to the surface of the Bessel cone makes an angle θ with the y-axis. Thus, the projection of the electric field E along the y-axis is $E_y = E\cos\theta$ and along the z-axis is $E_z = E\sin\theta$. For simple understanding, here, I can consider three radial coordinates as $r = (x^2 + y^2)^{1/2}$, $\nu = (y^2 + z^2)^{1/2}$, and $\rho = (x^2 + z^2)^{1/2}$. Each k-vector on the Bessel cone has a unique plane of incidence, and this plane of incidence linearly changes in the azimuthal direction as a function of ϕ. As a result, the azimuthal polarization-dependent plane of incidence splits the BB into s-polarized and p-polarized components, even though the scalar BB has a single linear polarization. With respect to the Bessel cone surface, while p-polarization is oscillating normal to the surface, the oscillation of s-polarization is tangential to the surface. Therefore, in the process of a linearly polarized plane wave being transformed into a conical-shape beam, the polarization distribution sees a twist along the azimuthal direction similar to optical polarization Möbius strips [34]. The twist in the polarization distribution can be enhanced via creating a large Bessel cone angle. For a given Bessel cone angle (θ) and for vertical polarization along the y-axis, BB sees zero polarization twist at an azimuthal angle $\phi = 0$ and π, and maximum polarization twist of cos θ at $\phi = \pi/2$ and $3\pi/2$. With reference to the plane of incidence on the conical surface, s-polarization and p-polarization are orthogonal to each other. Also, the Bessel cone angle θ splits the amplitude of BB into transverse and longitudinal components, and these components are also a function of azimuthal angle ϕ.

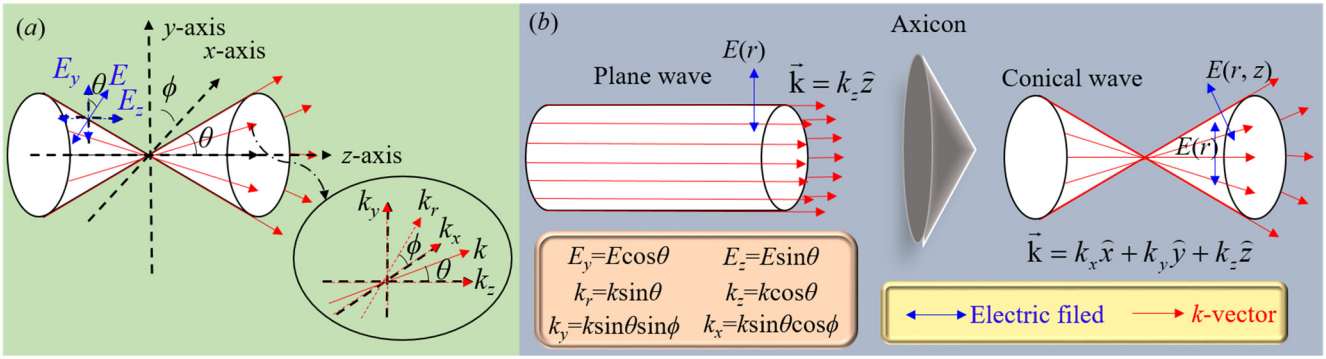

Figure 1. Vector diagram of a Bessel beam whose polarization is in yz-plane: (**a**) Propagation vector and electric field vector of Bessel beam along the x-, y-, and z-axes. (**b**) Optical field distribution of the Bessel beam formed by pumping a vertically polarized plane wave to an axicon. The red arrows correspond to the k-vector and the blue color double arrows represent electric field oscillation.

The optical field distribution of BB can be understood in its cross-section, as depicted in Figure 1b. A plane wave, linearly polarized along the y-axis and propagating along the z-axis, is passed through an axicon and converted into a BB. Now, this BB has polarization along the y- and z-axes due to the angular propagation of individual waves with respect to the z-axis. Within the BB, while the waves in the yz-plane are p-polarized, waves that are present in the xz-plane have s-polarization. The rest of the waves have p-polarization

and *s*-polarization components. The *s*-polarized and *p*-polarized components of the optical field at an arbitrary position (r, ϕ) can be written in terms of azimuthal angle ϕ. Here, the angle ϕ is considered to be from the *x*-axis. It is also noted that the propagation vector *k* of individual waves has three components k_x, k_y, and k_z along the respective *x*-, *y*-, and *z*-axes, whereas the BB has only one propagation vector component along the *z*-axis (k_z). This scenario can be understood as follows: The circular symmetry of the BB produces cancellation of the *x*- and *y*-components of *k*-vectors, which are propagating at opposite points on the Bessel cone. As a result, the effective *k*-vectors along the *x*- and *y*-directions are zero. In the case of *z*-component of the *k*-vector, all the projections of the *k*-vector are along a single *z*-direction and the resultant *k*-vector is along the *z*-axis with a non-zero value.

The information discussed above on the three-dimensional polarization distribution of BBs can be further expressed and understood in terms of mathematical equations. The total optical field of BB can be split into the optical field components along the *s*-polarization, *p*-polarization, transverse polarization, and longitudinal polarization. First of all, the optical field amplitude and intensity of the BB can be written in terms of *s*-polarized and *p*-polarized components as

$$\vec{E} = \vec{E}_s(y, \varphi) + \vec{E}_p(y, z, \varphi) \tag{1}$$

with

$$\vec{E}_s(y, \varphi) = \vec{E}\cos\varphi \& \vec{E}_p(y, z, \varphi) = \vec{E}\sin\varphi.$$

The total intensity distribution in terms of *s*-polarized and *p*-polarized components is given by

$$I = \left|\vec{E}\right|^2 = I_s(r, \varphi) + I_p(r, \varphi) \tag{2}$$

with

$$I_s(y, \varphi) = I\cos^2\varphi \& I_p(y, z, \varphi) = I\sin^2\varphi.$$

Moreover, the optical field amplitude and intensity of BB can be expressed in terms of the transverse optical field E_t and longitudinal optical field E_z as

$$\vec{E} = \vec{E}_t(y, \varphi, \theta) + \vec{E}_z(z, \varphi, \theta) \tag{3}$$

with

$$\vec{E}_t(y, \varphi, \theta) = \vec{E}_s + \vec{E}_p\cos\theta \& \vec{E}_z(z, \varphi, \theta) = \vec{E}_p\sin\theta$$

and the corresponding intensity distribution is given by

$$I = \left|\vec{E}\right|^2 = I_t(y, \varphi, \theta) + I_z(z, \varphi, \theta) \tag{4}$$

with

$$I_t(y, \varphi, \theta) = I_s + I_p\cos^2\theta \& I_z(z, \varphi, \theta) = I_p\sin^2\theta.$$

Furthermore, a vertically polarized optical field of a plane wave transformed into a vertically and longitudinally polarized optical field while it is converted into a BB in the presence of an axicon can be visualized in the following equation as

$$\underbrace{E|y\rangle}_{\text{plane wave}} \xrightarrow{\text{Axicon}} \underbrace{\overbrace{\overbrace{E\cos\varphi|y\rangle}^{E_{st}}}^{E_s} + \overbrace{E\sin\varphi\left[\overbrace{\cos\theta|y\rangle}^{E_{pt}} + \overbrace{\sin\theta|z\rangle}^{E_{pz}}\right]}^{E_p}}_{\text{Bessel beam}}. \tag{5}$$

Here, the unit vectors along the x, y, and z coordinates in the ket form are $|x\rangle = (1\ 0\ 0)^{\mathrm{T}}$, $|y\rangle = (0\ 1\ 0)^{\mathrm{T}}$, and $|z\rangle = (0\ 0\ 1)^{\mathrm{T}}$. The inner product of Equation (5) with its complex conjugate $\langle \cdot | \cdot \rangle$ provides the corresponding intensity distribution in each polarization state as

$$\underbrace{I}_{\text{plane wave}} \xrightarrow{\text{Axicon}} \underbrace{\overbrace{I\cos^2\varphi}^{E_s}}_{E_{st}} + \overbrace{I\sin^2\varphi\left[\overbrace{\cos^2\theta}^{E_{pt}} + \overbrace{\sin^2\theta}^{E_{pz}}\right]}^{E_p}. \quad (6)$$

Bessel beam

3. Results and Discussion

The s-polarized, p-polarized, transverse polarized, and longitudinal polarized components of the BB (provided by Equation (6)) are given in Figure 2. The intensity of the BB is equally distributed between s-polarization and p-polarization, and this is true for any Bessel cone angle. These components uniformly vary in the azimuthal direction. Additionally, the intensity of the BB is unequally distributed between transverse and longitudinal polarization components. The intensity in the longitudinal component is always less than the intensity in the transverse component, and this asymmetry in the intensity distribution increases when the angle of the Bessel cone is decreased. The unequal intensity distribution between transverse and longitudinal components can be understood through s- and p-polarizations. While s-polarization has only transverse intensity, p-polarization has both transverse and longitudinal intensities (see Equation (6)). It is also noted that the longitudinal component of the BB can be successfully neglected for a few degrees of the Bessel cone angle. Various techniques have been used to demonstrate BBs with larger cone angles [35–39]. These larger cone angle BBs have a significant longitudinal component and can play a pivotal role in modern light-based applications. When a BB is normally incident on the materials for the study of light–matter interactions, we can directly use the intensity distributions given in Figure 2. However, in the case of oblique incidence, the intensity lobes created in the four polarization states will have an asymmetric intensity distribution. Hence, in oblique incidence, we must consider the angle of incidence of a BB in the simulation work to prevent artifacts in the experimental data analysis of light–matter interactions.

The non-uniform intensity distribution produced in the four polarization components of BBs is prominent for large Bessel cone angles. Especially for tight-focusing BB polarization-dependent applications, we must prevent polarization-dependent intensity modulations across the beam's cross-section. We can overcome this drawback by superposition of two collinearly propagating orthogonally polarized identical BBs of the same intensity. To understand this scenario, we can generate a BB that is orthogonal to the BB given by Equation (6) via pumping a horizontally polarized light to an axicon. The resultant optical field amplitude and intensity are given by

$$\underbrace{E|x\rangle}_{\text{plane wave}} \xrightarrow{\text{Axicon}} \underbrace{\overbrace{E\sin\varphi|x\rangle}^{E_s}}_{E_{st}} + \overbrace{e^{i\pi/2}E\cos\varphi\left[\overbrace{\cos\theta|x\rangle}^{E_{pt}} + \overbrace{\sin\theta|z\rangle}^{E_{pz}}\right]}^{E_p}, \quad (7)$$

Bessel beam

$$\underbrace{I}_{\text{plane wave}} \xrightarrow{\text{Axicon}} \overbrace{\overbrace{I\sin^2\varphi}^{E_s} + \overbrace{I\cos^2\varphi\left[\overbrace{\cos^2\theta}^{E_{pt}} + \overbrace{\sin^2\theta}^{E_{pz}}\right]}^{E_p}}^{\text{Bessel beam}}. \quad (8)$$

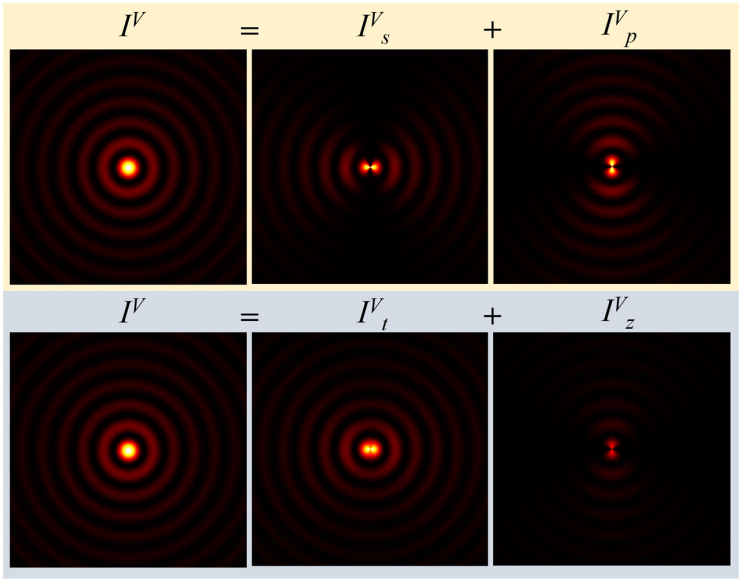

Figure 2. The total intensity of the Bessel beam and its intensity (**first row**) in *s*-polarization and *p*-polarization and (**second row**) in transverse polarization and longitudinal polarization (cone angle of Bessel beam used is 40°). Here, superscript V on intensity I is used for the representation of vertical polarization.

From Equations (5) and (7), the intensity distribution of a BB formed by the superposition of two orthogonal linear polarized plane waves pumped to the axicon is

$$\underbrace{I^H + I^V}_{\text{plane wave}} = \xrightarrow{\text{Axicon}} \overbrace{\overbrace{I^H\sin^2\varphi + I^V\cos^2\varphi}^{E_s} + \overbrace{\left(I^H\cos^2\varphi + I^V\sin^2\varphi\right)\left[\overbrace{\cos^2\theta}^{E_{pt}} + \overbrace{\sin^2\theta}^{E_{pz}}\right]}^{E_p}}^{\text{Bessel beam}}. \quad (9)$$

Here, I^H and I^V are used, respectively, for horizontally and vertically polarized light intensities for their identification. As shown in Figure 3, from Equation (9), I can create a uniform intensity in the BB's cross-section for four polarization components. This technique is cost-effective and simple for preventing polarization-dependent effects on a BB. The three-dimensional polarization distribution with uniform light intensity created by the superposition of two orthogonally polarized BBs can see tremendous applications in modern material engineering technology. For instance, the presence of longitudinal polarization in Rb atoms is strongly coupled to a whispering-gallery-mode micro-resonator that fundamentally alters the interaction between light and matter [40]. The three-dimensional polarization created under tight focusing can be woven into loops, links, knots, and Möbius strips [41–43]. Three-dimensional polarization distribution has been utilized for gold nanorods for orientation-unlimited polarization encryption with ultra-security [44]. We can

also create three-dimensional polarization textures in polarization-sensitive absorptive materials like azo-polymers [45].

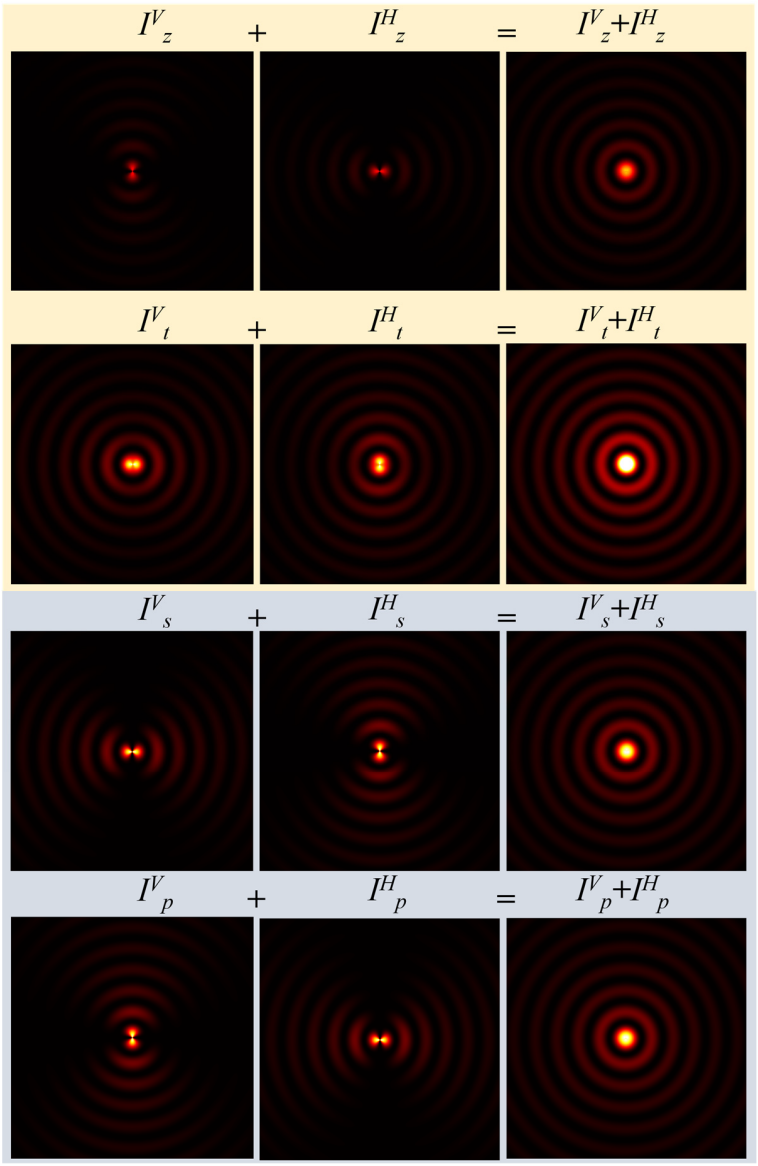

Figure 3. The intensity of longitudinal and transverse components of vertically and horizontally polarized Bessel beams.

The *s*-polarization and *p*-polarization components of BB are equivalent to the linearly polarized first-order Hermite–Gaussian modes in Laguerre–Gaussian-based vector beam generation. By the superposition of two orthogonally linear polarized BBs, we can straightforwardly generate cylindrical vector BBs in *s*-polarization and *p*-polarization. The expression for the superposition state is given by

$$\psi_j(\varphi) = \frac{E_j^H}{\sqrt{2}} e^{-i\varphi/2} + \frac{E_j^V}{\sqrt{2}} e^{i\varphi/2}, \tag{10}$$

where φ is the phase delay between the two orthogonally linear polarized BBs and j stands for *s*-polarization and *p*-polarization. As shown in Figure 4, we can generate four well-known types of vector modes [46,47] in the zero-order BB, which have central bright intensity. The four types of vector modes created in BBs are given in the white insets

of Figure 4. The black double arrow represents the state of polarization. As shown in Figure 5, we can also generate vector vortex modes in *s*-polarization and *p*-polarization by the superposition of higher-order BBs with orthogonal polarization. Any particular type of vector beam in *s*-polarization and *p*-polarization can be generated in a controlled manner by providing the required phase delay φ between the two collinearly propagating BBs with orthogonal polarizations. While type I and type II vector modes are created in *s*-polarization at respective phase delays of $\varphi = \pi$ and 0, type III and type IV vector modes are produced in *p*-polarization at respective phase delays of $\varphi = 0$ and π. For the rest of the phase delays, the vector modes have elliptical polarization. It is also noted that irrespective of BB's order, the vector modes created in *s*-polarization and *p*-polarization are first-order V-point singularity vector modes with Poincaré–Hopf index of $\eta = \pm 1$.

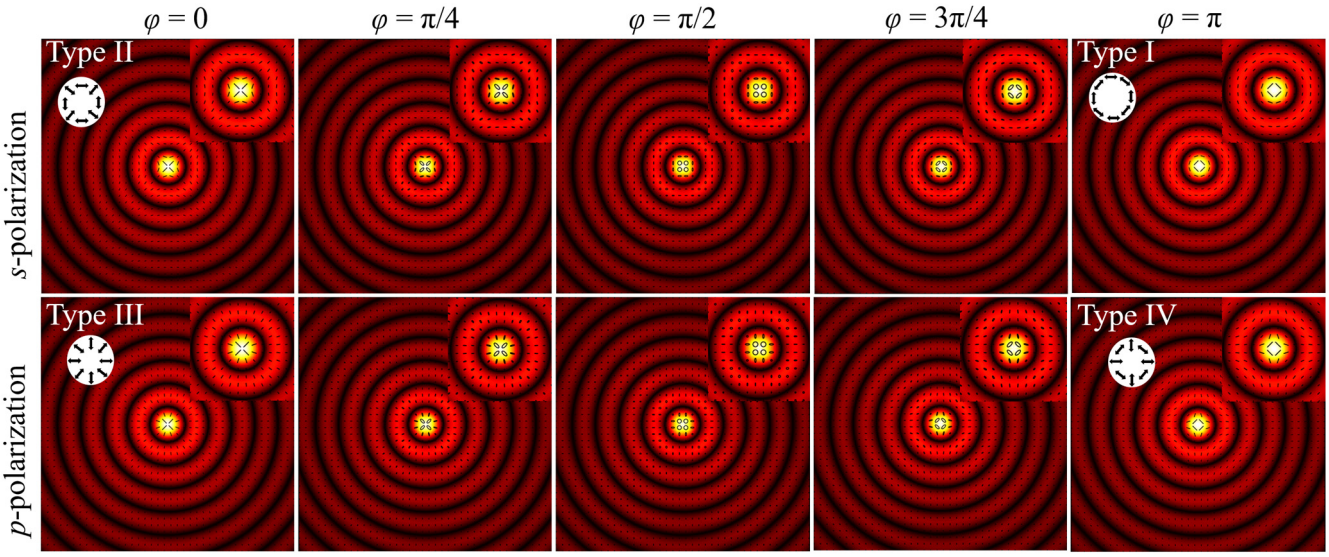

Figure 4. Different types of vector Bessel beams are generated in *s*-polarization and *p*-polarization by the superposition of two orthogonally linear polarized zero-order scalar Bessel beams. The four types of vector modes created in *s*-polarization and *p*-polarization are given in white insets. Also, the central part of the vector BB is enlarged and given in the left-side inset for all the images.

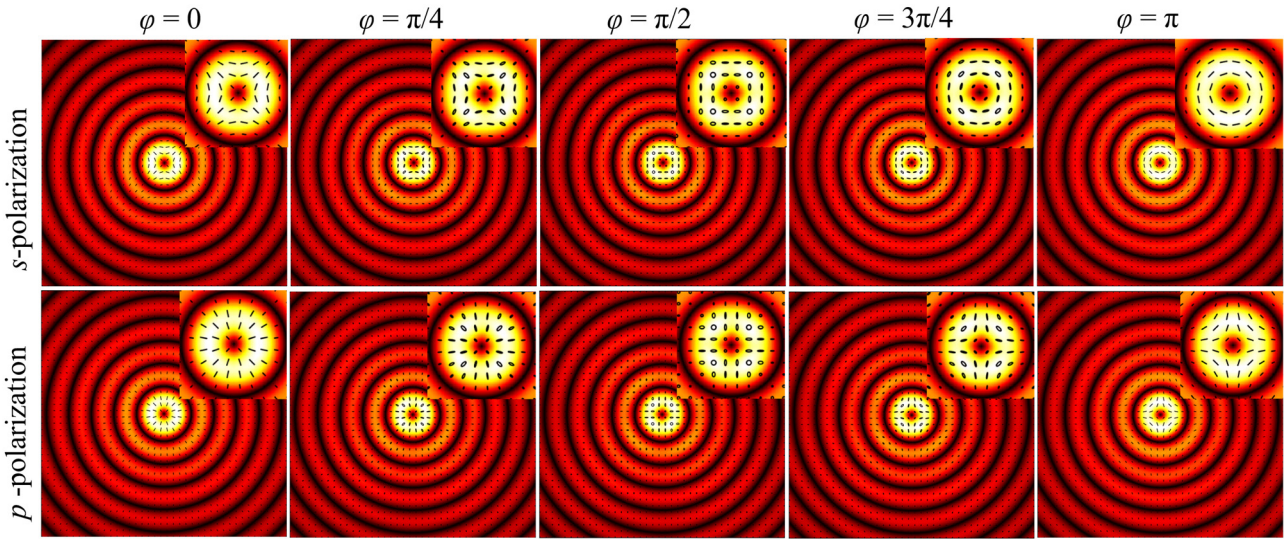

Figure 5. Various types of vector Bessel beams are generated in *s*-polarization and *p*-polarization by the superposition of two orthogonally linear polarized first-order scalar Bessel beams. The central part of the vector BB is enlarged and given in the left-side inset for all the images.

As depicted in Figure 6, the optical field is distributed between *p*-polarization and *s*-polarization and is a function of the azimuthal angle. Any physical phenomenon that is a function of *p*-polarization and *s*-polarization can modulate the cross-sectional intensity distribution of a BB in a similar way, as shown in Figure 6. The Fresnel reflection losses at the interface due to *s*-polarization and *p*-polarization components produce profound changes in the cross-section of the BB. Hence, whenever we use a BB in applications, we must consider its reflection and transmission losses at the interface of mediums for *s*-polarization and *p*-polarization components. For example, some of the diffractive optical elements, like beam splitters, mirrors, lenses, etc. have a polarization-dependent nature in their functioning.

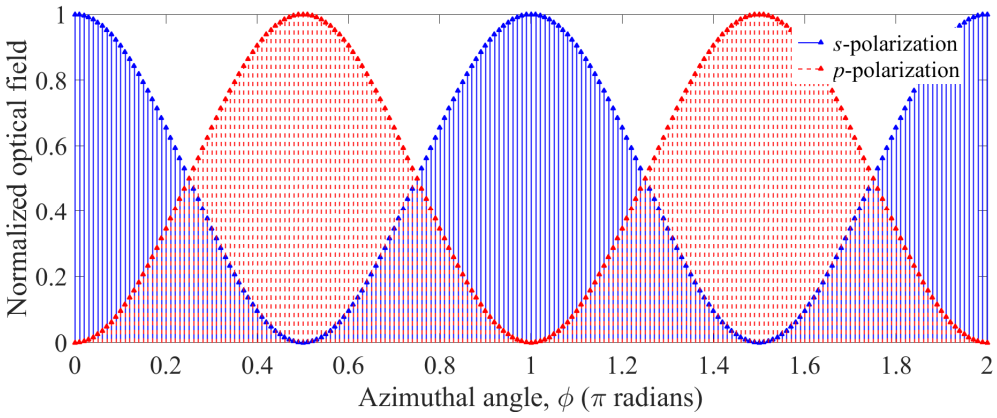

Figure 6. Optical field distribution in *p*-polarization and *s*-polarization in the azimuthal direction.

The incident BB's amplitude of E_i from medium 1 of the refractive index n_1 incident on the interface formed by medium 2 of the refractive index n_2 is split into the transmitted amplitude of E_t and reflected amplitude of E_r. These three amplitudes can be written in terms of their *s*-polarization and *p*-polarization components under the constraints formed by reflective and transitive coefficients at the interface of the two mediums as

$$\vec{E}_i = \vec{E}_s(y,\varphi) + \vec{E}_p(y,z,\varphi), \tag{11a}$$

$$\vec{E}_r = r_s\vec{E}_s(y,\varphi) - r_p\vec{E}_p(y,z,\varphi), \tag{12b}$$

$$\vec{E}_t = t_s\vec{E}_s(y,\varphi) + t_p\vec{E}_p(y,z,\varphi). \tag{13c}$$

The polarization-dependent Fresnel reflection and transmission coefficients are given by

$$r_s = \frac{n_1\cos\theta_1 - n_2\cos\theta_2}{n_1\cos\theta_1 + n_2\cos\theta_2}, \tag{12a}$$

$$t_s = \frac{2n_1\cos\theta_1}{n_1\cos\theta_1 + n_2\cos\theta_2}, \tag{12b}$$

$$r_p = \frac{n_2\cos\theta_1 - n_1\cos\theta_2}{n_2\cos\theta_1 + n_1\cos\theta_2}, \tag{12c}$$

$$t_p = \frac{2n_1\cos\theta_1}{n_2\cos\theta_1 + n_1\cos\theta_2}. \tag{12d}$$

Here, θ_1 and θ_2 are the angles of the Bessel cone in medium 1 and medium 2. The Bessel cone angle in medium 2 is in terms of the incident Bessel cone angle given by $\theta_2 = \sin^{-1}[(n_1\sin\theta_1)/n_2]$. While the *s*-polarization and *p*-polarization components are in-phase in the transmission, they can have some phase difference ($\Delta\varphi_{sp}$) in the reflection. Hence,

the transverse intensity distribution of the reflected component depends on $\Delta\varphi_{sp}$. Also, the phase difference ($\Delta\varphi_{sp}$) depends on the Bessel cone angle. For example, in the case of $n_1/n_2 = 1.5$, $\Delta\varphi_{sp} = 0$ for $\theta_1 < \theta_p$ (polarization angle) and $\Delta\varphi_{sp} = \pi$ for $\theta_1 \geq \theta_p$. Hence, here, the asymmetry can account for the dependency of the Fresnel reflection and transmission coefficients on the Bessel cone angle for the *s*-polarization and *p*-polarization components in the BBs.

The details on the transmission and reflection of the BB at the interface formed by two mediums of relative refractive index $n_1/n_2 = 1/1.5$ are presented in Figure 7. The transmittance and reflectance for *s*-polarization and *p*-polarization components vary with the Bessel cone angle differently, which leads to the unequal intensity of *s*-polarization and *p*-polarization components in the BB. The relative change in Fresnel reflection losses for *s*-polarization and *p*-polarization components increases with the Bessel cone angle. The changes in the transverse intensity distribution of the BB while it is transmitted and reflected for its Bessel cone angles $\theta = 25^\circ$ and 50° are shown in Figure 7c,d, respectively. For any relative refractive index, the Fresnel reflection losses are minimal for a lower Bessel cone angle. Hence, the effect of reflection losses on BBs with few degrees of cone angle is successfully neglected. However, as the Bessel cone angle increases, the cross-sectional intensity distribution of the BB illustrates significant distortions and no longer represents similar features of an incident BB. These distortions are prominent in the reflected beam compared with the transmitted beam due to the very low reflected intensity, which is comparable with the intensity distortions created by the interface. In the case of higher-order BBs, the quantity of the OAM and the quality of the helical wave front cannot be preserved when they see a change in the refractive index.

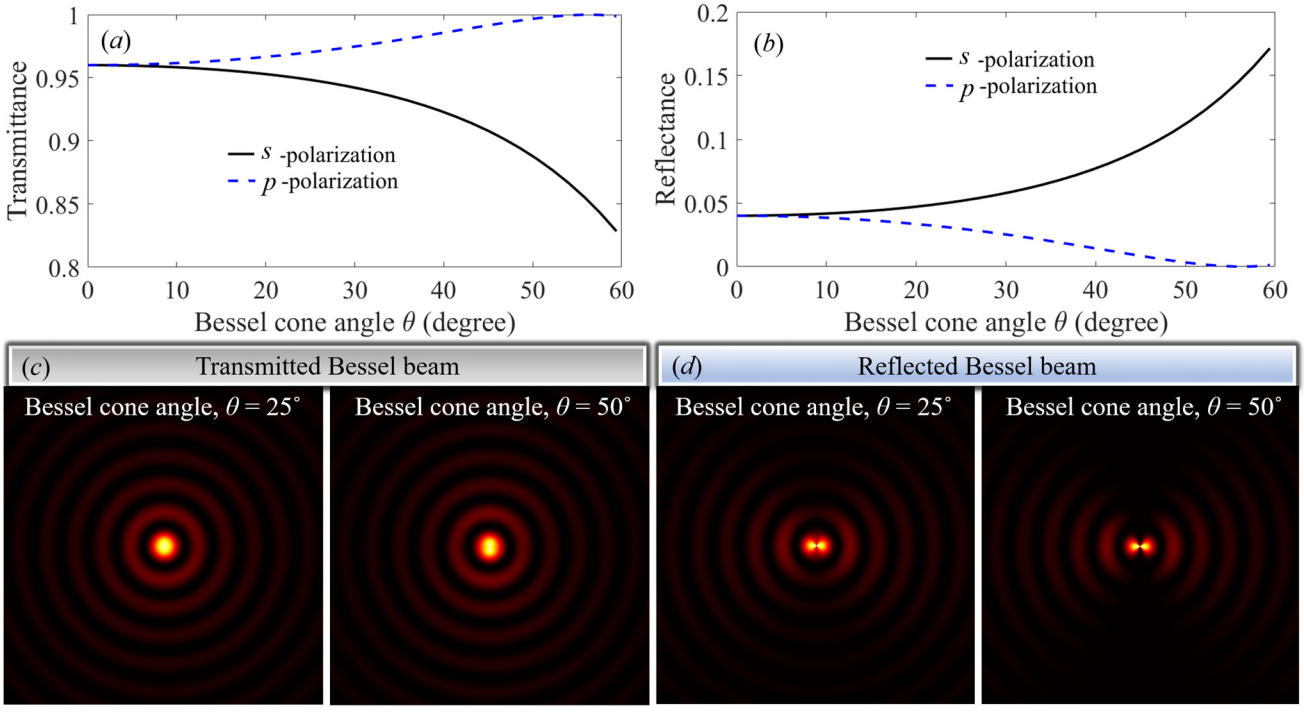

Figure 7. The intensity modulation in the Bessel beam while it is propagating through the interface formed by two mediums of relative refractive index $n_1/n_2 = 1/1.5$: (**a**) transmittance and (**b**) reflectance of Bessel beam at the interface. The transverse intensity distribution of the Bessel beam while it is (**c**) transmitted and (**d**) reflected at the interface. Here, the intensity distribution in the beam cross-section is self-normalized with its peak intensity.

Another illustration of Fresnel refraction is the change in the spot size of the BB. In the presence of a normal incidence of a BB from one isotropic medium to another isotropic medium, the spot size changes based on the relative refractive index but there will be no

effect on its circular shape. However, in the case of oblique incidence, the circular shape of a BB changes to an elliptical shape because the incident angle of individual waves is different. For a higher-order BB, the oblique incidence can split its vorticity. In the case of oblique incidence, the angles θ_1 and θ_2 change in the azimuthal direction due to the incidence angle θ_0 of the BB. It is also noted that the above discussion is not true for anisotropic mediums. The anisotropy in the refractive index distorts the traverse intensity and phase distributions of BBs, even in normal incidence [48–50].

We can create evanescent BBs by providing large $k_r > k$ [51], and they can be experimentally realized by tight focusing of BBs [52]. The evanescent BB has a strong longitudinal component compared with the transverse component, which is very useful in near-field optical experiments like surface plasmon resonance and near-field optical microscopes [25]. A linearly polarized evanescent BB sees the asymmetric intensity distribution due to the difference in the reflection coefficient of *s*-polarization and *p*-polarization components. However, this asymmetry was successfully removed with radially polarized BBs [26]. Here, I suggest that the superposition of two orthogonally polarized identical BBs can be used cost-effectively to prevent asymmetry in the evanescent BBs. Also, the superposition of two orthogonally linear polarized BBs can replace radial polarized BBs in the generation of cylindrical symmetric micro-size needle structures under tight focusing configurations [53–55].

My model can be further extended to explain the polarization properties of the structured modes, whose transverse intensity distribution follows the Bessel function [56–60]. For application purposes, the wavelength of BBs can be tuned through nonlinear-wave mixing, which is polarization-dependent [61–63]. The nonlinear wave-mixing of BBs not only tunes the wavelength but also changes their order (this is not true for a zero-order BB). In the case of tight-focusing BBs, we must know their polarization distribution for their wavelength tuning. One can use my analysis to understand and rectify the polarization effects on the wavelength tuning of BBs.

We can experimentally realize the theoretical results provided in Figures 4 and 5 by using two collinearly propagating BBs with orthogonal polarization, which we can create with the Mach–Zander Interferometer (MZI). As depicted in Figure 8, the combination of a half-wave plate and the first polarizing beam splitter (PBS) can be employed to generate two collimated laser beams that have equal intensity but are orthogonally polarized. The two orthogonally polarized beams can again be combined through the second PBS to create two collinearly propagating laser beams with orthogonal polarizations. The resultant beam can be pumped to an axicon to create two superposed zero-order BBs with orthogonal polarization. The phase delay φ between the two BBs can be controlled by the delay line provided by mirrors M_3–M_6 in the MZI. Further, we can generate higher-order BBs from the same experimental configuration by simply inserting a spiral phase plate before the first PBS. The superposed orthogonally polarized BBs produce V-point singularity vector modes in *s*-polarization and *p*-polarization. However, the total polarization state of this superposition is a vector beam with uniform elliptical polarization. The state of elliptical polarization depends on the phase delay φ. Here, φ produces polarization Lissajous figures [64], as shown in Figures 4 and 5. For example, we can produce diagonal, circular, and anti-diagonal polarization states at respective values of $\varphi = 0, \pm\pi/2$, and π.

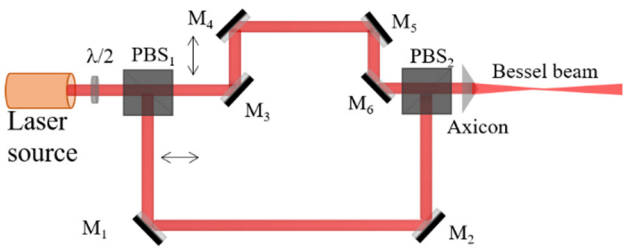

Figure 8. Experimental configuration can be used to generate various cylindrical vector modes in *s*-polarization and *p*-polarization. Here, PBS_i is the polarizing beam splitter, M_i is the mirror, and $\lambda/2$ is the half-wave plate. The double arrows in the experimental setup represent the polarization direction.

4. Conclusions

I have presented the properties of BBs in *s*-polarization, *p*-polarization, transverse polarization, and longitudinal polarization, explaining why these beams are divided into four polarization components and showing how to overcome the non-uniform intensity distribution created in the four polarization components. Moreover, I extended my analysis to reconstruct uniform intensity distribution and vector modes in the four polarization components by controlling input parameters, giving some concrete examples, and discussing their symmetries. By numerical illustration, I have shown that these modes can exhibit all four types of cylindrical vector modes. A simple MZI can experimentally realize the theoretically suggested modes. My theoretical analysis provides not only remarkable insight into but also greatly simplifies polarization effects in the BBs' propagation.

Funding: This research received no external funding.

Institutional Review Board Statement: Not applicable.

Informed Consent Statement: Not applicable.

Data Availability Statement: Not applicable.

Conflicts of Interest: The author declares no conflict of interest.

References

1. Durnin, J. Exact solutions for nondiffracting beams. I. The scalar theory. *JOSA A* **1987**, *4*, 651–654. [CrossRef]
2. Durnin, J.; Miceli, J.J., Jr.; Eberly, J.H. Diffraction-free beams. *Phys. Rev. Lett.* **1987**, *58*, 15. [CrossRef] [PubMed]
3. Gori, F.; Guattari, G.; Padovani, C. Bessel-gauss beams. *Opt. Commun.* **1987**, *64*, 491–495. [CrossRef]
4. Li, Y.; Lee, H.; Wolf, E. New generalized Bessel–Gaussian beams. *JOSA A* **2004**, *21*, 640–646. [CrossRef]
5. Khan, S.A. Cross polarization in Gaussian and Bessel light beams. *Opt. Commun.* **2023**, *545*, 129728. [CrossRef]
6. Mishra, S.R. A vector wave analysis of a Bessel beam. *Opt. Commun.* **1991**, *85*, 159–161. [CrossRef]
7. McGloin, D.; Dholakia, K. Bessel beams: Diffraction in a new light. *Contemp. Phys.* **2005**, *46*, 15–28. [CrossRef]
8. Rao, A.S.; Samanta, G.K. On-axis intensity modulation-free, segmented, zero-order Bessel beams with tunable ranges. *Opt. Lett.* **2018**, *43*, 3029–3032. [CrossRef]
9. Chattrapiban, N.; Rogers, E.A.; Cofield, D.; Hill, W.T., III; Roy, R. Generation of nondiffracting Bessel beams by use of a spatial light modulator. *Opt. Lett.* **2003**, *28*, 2183–2185. [CrossRef]
10. Chen, B.; Huang, X.; Gou, D.; Zeng, J.; Chen, G.; Pang, M.; Hu, Y.; Zhao, Z.; Zhang, Y.; Zhou, Z.; et al. Rapid volumetric imaging with Bessel-Beam three-photon microscopy. *Biomed. Opt. Exp.* **2018**, *9*, 1992–2000. [CrossRef]
11. Garcés-Chávez, V.; McGloin, D.; Melville, H.; Sibbett, W.; Dholakia, K. Simultaneous micromanipulation in multiple planes using a self-reconstructing light beam. *Nature* **2002**, *419*, 145–147. [CrossRef] [PubMed]
12. Bhuyan, M.K.; Somayaji, M.; Mermillod-Blondin, A.; Bourquard, F.; Colombier, J.P.; Stoian, R. Ultrafast laser nanostructuring in bulk silica, a "slow" microexplosion. *Optica* **2017**, *4*, 951–958. [CrossRef]
13. Arita, Y.; Lee, J.; Kawaguchi, H.; Matsuo, R.; Miyamoto, K.; Dholakia, K.; Omatsu, T. Photopolymerization with high-order Bessel light beams. *Opt. Lett.* **2020**, *45*, 4080–4083. [CrossRef] [PubMed]
14. Lu, Z.; Guo, Z.; Fan, M.; Guo, M.; Li, C.; Yao, Y.; Zhang, H.; Lin, W.; Liu, H.; Liu, B. Tunable Bessel Beam Shaping for Robust Atmospheric Optical Communication. *J. Light. Technol.* **2022**, *40*, 5097–5106. [CrossRef]
15. Hecht, E. *Optics*, 4th ed.; Pearson Education: San Francisco, CA, USA, 2001; pp. 121–133.
16. Li, H.; Honary, F.; Wang, J.; Liu, J.; Wu, Z.; Bai, L. Intensity, phase, and polarization of a vector Bessel vortex beam through multilayered isotropic media. *Appl. Opt.* **2018**, *57*, 1967–1976. [CrossRef]
17. Mugnai, D. Propagation of Bessel beams from a dielectric to a conducting medium. *Appl. Opt.* **2011**, *50*, 2654–2658. [CrossRef]
18. Mugnai, D. Bessel beam through a dielectric slab at oblique incidence: The case of total reflection. *Opt. Commun.* **2002**, *207*, 95–99. [CrossRef]
19. Wang, J.J.; Wriedt, T.; Lock, J.A.; Jiao, Y.C. General description of transverse mode Bessel beams and construction of basis Bessel fields. *J. Quant. Spect. Rad. Trans.* **2017**, *195*, 8–17. [CrossRef]
20. Novitsky, A.V.; Barkovsky, L.M. Vector Bessel beams in bianisotropic media. *J. Opt. A Pure Appl. Opt.* **2005**, *7*, 550. [CrossRef]
21. Manela, O.; Segev, M.; Christodoulides, D.N. Nondiffracting beams in periodic media. *Opt. Lett.* **2005**, *30*, 2611–2613. [CrossRef]
22. Novitsky, A.V.; Barkovsky, L.M. Total internal reflection of vector Bessel beams: Imbert–Fedorov shift and intensity transformation. *J. Opt. A Pure Appl. Opt.* **2008**, *10*, 075006. [CrossRef]
23. Simon, R.; Sudarshan, E.C.G.; Mukunda, N. Cross polarization in laser beams. *Appl. Opt.* **1987**, *26*, 1589–1593. [CrossRef] [PubMed]
24. Sheppard, C.J.; Rehman, S.; Balla., N.K.; Yew., E.Y.; Teng, T.W. Bessel beams: Effects of polarization. *Opt. Commun.* **2009**, *282*, 4647–4656. [CrossRef]

25. Chen, W.; Zhan, Q. Realization of an evanescent Bessel beam via surface plasmon interference excited by a radially polarized beam. *Opt. Lett.* **2009**, *34*, 722–724. [CrossRef] [PubMed]
26. Zhan, Q. Evanescent Bessel beam generation via surface plasmon resonance excitation by a radially polarized beam. *Opt. Lett.* **2006**, *31*, 1726–1728. [CrossRef] [PubMed]
27. Rao, A.S.; Morohashi, T.; Kerridge-Johns, W.R.; Omatsu, T. Generation of higher-order Laguerre–Gaussian modes from a diode-pumped Pr 3+: LiYF 4 laser with an intra-cavity spherical aberration. *JOSA B* **2023**, *40*, 406–411. [CrossRef]
28. Boley, C.D.; Rubenchik, A.M. Modeling of laser interactions with composite materials. *Appl. Opt.* **2013**, *52*, 3329–3337. [CrossRef]
29. Kobayashi, M.; Minár, J.; Khan, W.; Borek, S.; Hai, P.N.; Harada, Y.; Schmitt, T.; Oshima, M.; Fujimori, A.; Tanaka, M.; et al. Minority-spin impurity band in n-type (In, Fe) As: A materials perspective for ferromagnetic semiconductors. *Phys. Rev. B* **2021**, *103*, 115111. [CrossRef]
30. Lio, G.E.; Ferraro, A.; Kowerdziej, R.; Govorov, A.O.; Wang, Z.; Caputo, R. Engineering Fano-Resonant Hybrid Metastructures with Ultra-High Sensing Performances. *Adv. Opt. Mat.* **2023**, *2023*, 2203123. [CrossRef]
31. Gong, Y.; Hu, M.; Harris, N.; Yang, Z.; Xie, T.; Teklu, A.; Kuthirummal, N.; Koenemann, J.; Xu, X.; Cheong, S.W.; et al. Strong laser polarization control of coherent phonon excitation in van der Waals material Fe3GeTe2. *npj 2D Mat. Appl.* **2022**, *6*, 9. [CrossRef]
32. Mugnai, D.; Spalla, P. Electromagnetic propagation of Bessel-like localized waves in the presence of absorbing media. *Opt. Commun.* **2009**, *282*, 4668–4671. [CrossRef]
33. Yang, B.; Ouyang, M.; Ren., H.; Wu, J.; Zhang., Y.; Fu, Y. January. Polarization-Dependent Absorption and Transmission Metasurfaces for Linearly and Circularly Polarized Light in Terahertz Band. *Photonics* **2023**, *10*, 100. [CrossRef]
34. Garcia-Etxarri, A. Optical polarization mobius strips on all-dielectric optical scatterers. *ACS Photonics* **2017**, *4*, 1159–1164. [CrossRef]
35. Matsuoka, Y.; Kizuka, Y.; Inoue, T. The characteristics of laser micro drilling using a Bessel beam. *Appl. Phys. A* **2006**, *84*, 423–430. [CrossRef]
36. Belloni, V.V.; Froehly, L.; Billet, C.; Furfaro, L.; Courvoisier, F. Generation of extremely high-angle Bessel beams. *Appl. Opt.* **2023**, *62*, 1765–1768. [CrossRef]
37. Milne, G.; Jeffries, G.; Chiu, D. Tunable generation of Bessel beams with a fluidic axicon. *Appl. Phys. Lett.* **2008**, *92*, 261101. [CrossRef]
38. Boucher, P.; Del Hoyo, J.; Billet, C.; Pinel, O.; Labroille, G.; Courvoisier, F. Generation of high conical angle Bessel–Gauss beams with reflective axicons. *Appl. Opt.* **2018**, *57*, 6725–6728. [CrossRef]
39. Bergner, K.; Müller, M.; Klas, R.; Limpert, J.; Nolte, S.; Tünnerman, A. Scaling ultrashort laser pulse induced glass modifications for cleaving applications. *Appl. Opt.* **2018**, *57*, 5941–5947. [CrossRef]
40. Maucher, F.; Skupin, S.; Gardiner, S.A.; Hughes, I.G. Creating complex optical longitudinal polarization structures. *Phys. Rev. Lett.* **2018**, *120*, 163903. [CrossRef]
41. Larocque, H.; Sugic, D.; Mortimer, D.; Taylor, A.J.; Fickler, R.; Boyd, R.W.; Dennis, M.R.; Karimi, E. Reconstructing the topology of optical polarization knots. *Nat. Phys.* **2018**, *14*, 1079–1082. [CrossRef]
42. Bauer, T.; Banzer, P.; Karimi, E.; Orlov, S.; Rubano, A.; Marrucci, L.; Santamato, E.; Boyd, R.W.; Leuchs, G. Observation of optical polarization Möbius strips. *Science* **2015**, *347*, 964–966. [CrossRef]
43. Junge, C.; O'shea, D.; Volz, J.; Rauschenbeutel, A. Strong coupling between single atoms and nontransversal photons. *Phys. Rev. Lett.* **2013**, *110*, 213604. [CrossRef]
44. Li, X.; Lan, T.H.; Tien, C.H.; Gu, M. Three-dimensional orientation-unlimited polarization encryption by a single optically configured vectorial beam. *Nat. Commun.* **2012**, *3*, 998. [CrossRef]
45. Masuda, K.; Nakano, S.; Barada, D.; Kumakura, M.; Miyamoto, K.; Omatsu, T. Azo-polymer film twisted to form a helical surface relief by illumination with a circularly polarized Gaussian beam. *Opt. Express* **2017**, *25*, 12499–12507. [CrossRef]
46. Kumar, P.; Nishchal, N.K.; Omatsu, T.; Rao, A.S. Self-referenced interferometry for single-shot detection of vector-vortex beams. *Sci. Rep.* **2022**, *12*, 17253. [CrossRef]
47. Vyas, S.; Kozawa, Y.; Sato, S. Polarization singularities in super- position of vector beams. *Opt. Express* **2013**, *21*, 8972–8986. [CrossRef]
48. Zusin, D.H.; Maksimenka, R.; Filippov, V.V.; Chulkov, R.V.; Perdrix, M.; Gobert, O.; Grabtchikov, A.S. Bessel beam transformation by anisotropic crystals. *JOSA A* **2010**, *27*, 1828–1833. [CrossRef]
49. Riaud, A.; Thomas, J.L.; Baudoin, M.; Matar, O.B. Taming the degeneration of Bessel beams at an anisotropic-isotropic interface: Toward three-dimensional control of confined vortical waves. *Phys. Rev. E* **2015**, *92*, 063201. [CrossRef]
50. Khilo, N.A. Conical diffraction and transformation of Bessel beams in biaxial crystals. *Opt. Commun.* **2013**, *286*, 1–5. [CrossRef]
51. Ruschin, S.; Leizer, A. Evanescent bessel beams. *JOSA A* **1998**, *15*, 1139–1143. [CrossRef]
52. Grosjean, T.; Courjon, D.; Van Labeke, D. Bessel beams as virtual tips for near-field optics. *J. Micro.* **2003**, *210*, 319–323. [CrossRef] [PubMed]
53. Liu, T.; Tan, J.; Lin, J.; Liu, J. Generating super-Gaussian light needle of 0.36 λ beam size and pure longitudinal polarization. *Opt. Eng.* **2013**, *52*, 074104. [CrossRef]
54. Khonina, S.N.; Sergey, V.K.; Sergey, V.A.; Dmitry, A.S.; Janne, L.; Jari, T. Experimental demonstration of the generation of the longitudinal E-field component on the optical axis with high-numerical-aperture binary axicons illuminated by linearly and circularly polarized beams. *J. Opt.* **2013**, *15*, 085704. [CrossRef]

55. Dehez, H.; April, A.; Piché, M. Needles of longitudinally polarized light: Guidelines for minimum spot size and tunable axial extent. *Opt. Express* **2012**, *20*, 14891–14905. [CrossRef] [PubMed]
56. Allam, S.R.; Liu, L.; Cai, Y. Generating approximate non-diffractive three dimensional micro-size optical potentials by superposition. *Opt. Commun.* **2020**, *477*, 126297. [CrossRef]
57. Belyi, V.; Forbes, A.; Kazak, N.; Khilo, N.; Ropot, P. Bessel–like beams with z–dependent cone angles. *Opt. Eexpress* **2010**, *18*, 1966–1973. [CrossRef]
58. Allam, S.R. An intriguing interpretation of Cosine beams. *arXiv* **2023**, arXiv:2307.14201.
59. Porfirev, A.P.; Skidanov, R.V. Generation of an array of optical bottle beams using a superposition of Bessel beams. *Appl. Opt.* **2013**, *52*, 6230–6238. [CrossRef]
60. Rao, A.S.; Yadav, D.; Samanta, G.K. Nonlinear frequency conversion of 3D optical bottle beams generated using a single axicon. *Opt. Lett.* **2021**, *46*, 657–660. [CrossRef]
61. Wulle, T.; Herminghaus, S. Nonlinear optics of Bessel beams. *Phys. Rev. Lett.* **1993**, *70*, 10. [CrossRef]
62. Rao, A.S. Saturation effects in nonlinear absorption, refraction, and frequency conversion: A review. *Optik* **2022**, *267*, 169638.
63. Sutherland, R.L. *Handbook of Nonlinear Optics*, 2nd ed.; CRC Press: Boca Raton, FL, USA, 2003; pp. 33–120.
64. Włodarczyk, P.; Pustelny, S.; Budker, D. System for control of polarization state of light and generation of light with continuously rotating linear polarization. *Rev. Sci. Inst.* **2019**, *90*, 013110. [CrossRef] [PubMed]